Journal of Quantitative Spectroscopy & Radiative Transfer 151 (2015) 251–259

Contents lists available at ScienceDirect

Journal of Quantitative Spectroscopy & Radiative Transfer

journal homepage: www.elsevier.com/locate/jqsrt

Measurements of N_2-broadening and pressure-shift coefficients in the ν_3-band of $^{12}CH_4$ using a cw-OPO

Mohammad Jahjah [a], Linh Nguyen [a], Marco P. Moreno [a,b], Malo Cadoret [a,*], Jean-Jacques Zondy [a]

[a] Laboratoire Commun de Métrologie LNE-Cnam, 61 rue du Landy, 93210 La Plaine Saint-Denis, France
[b] Departamento de Física, Universidade Federal de Rondônia, Campus Ji-Paraná, Rondônia 76900-726, Brazil

ARTICLE INFO

Article history:
Received 28 July 2014
Received in revised form
26 September 2014
Accepted 3 October 2014
Available online 19 October 2014

Keywords:
Laser spectroscopy
Optical parametric oscillator
Line parameters
Methane

ABSTRACT

We have measured the nitrogen-collision-induced line broadening and line shift coefficients of three singlet lines – $P(1)$, $R(0)$ and $R(1)$ – belonging to the ν_3 band of methane ($^{12}CH_4$) at 3.29–3.32 μm using direct laser absorption spectroscopy by means of a continuous-wave mid-IR optical parametric oscillator. Owing to the well-isolated features of the singlet lines, the lineshapes were modeled with a simple Voigt profile in order to retrieve the line parameter coefficients. The values of the N_2-broadening and pressure-shift coefficients agree fairly well with the previously published ones that use either Fourier-transform or mid-infrared difference-frequency spectrometers along with more complex analytic spectroscopic models.

1. Introduction

Continuous-wave (cw) optical parametric oscillators (cw-OPOs) are becoming important spectroscopic tools in the short-wave mid-infrared (MIR) since the development of high-nonlinearity periodically poled ferroelectric materials in the mid-1990s. Their advantages include broadband spectral coverage (1.8–4.5 μm) thanks to quasi-phase-matching, narrow sub-MHz linewidth compared to quantum cascade lasers (few to tens of MHz), and convenient single-frequency tuning of the idler wave via pump frequency tuning when they are implemented as singly (signal-wave) resonant oscillators (SROs). Furthermore, SROs can provide high output power (~1 W) compared to, e.g. difference-frequency MIR laser sources, allowing them to be used in high-resolution molecular saturation spectroscopy. Doppler-free spectroscopy of the $F_2^{(2)}$ component of the $P(7)$ line of methane was among the first high-resolution spectroscopy applications of a pump-enhanced SRO [1]. More recently, several sub-Doppler (saturated absorption) spectroscopy experiments in the 3.3–3.4 μm of CH_4 and CH_3I were reported using cw-SROs [2–5].

In this paper, a home-designed fiber-laser-pumped SRO is used for the first time to measure N_2 collision-induced broadening and pressure-shift coefficients of the singlet lines $P(1)$, $R(0)$ and $R(1)$ lines located at 3009.011406 cm^{-1}, 3028.752260 cm^{-1} and 3038.498494 cm^{-1}, respectively, in the ν_3 band (fundamental C–H stretch bond) of methane. This OPO pumped at $\lambda_p \sim 1064$ nm demonstrated an extremely wide (~70 cm^{-1} at 3.3 μm) and rapid (4.5 THz/s) mode-hop-free idler frequency scan, capturing wide portions of the ν_3 band of methane in a single scan [6,7]. Recently this OPO source has been used to measure the linestrengths of the above singlet lines of CH_4 [8]. These singlet lines have been chosen so as to avoid interfering lines from multiplet manifolds with higher rotational quantum number J'' when the pressure is increased and to avoid line mixing effects, which require complex multi-line analysis [9].

Methane is known as one of the major greenhouse gases on Earth [10] and a minor constituent of the

* Corresponding author.
E-mail address: malo.cadoret@cnam.fr (M. Cadoret).

http://dx.doi.org/10.1016/j.jqsrt.2014.10.006
0022-4073/

atmospheres of Jupiter [11], Mars [12] and Titan [13]. The accurate knowledge of its spectroscopic parameters like self- and foreign-gas pressure-broadening and pressure-induced line shift coefficients is extremely useful for the interpretation and modeling of high-resolution infrared spectra of terrestrial and planetary atmospheres. Therefore, it is not surprising that many works have reported on these spectral parameters for the numerous ro-vibrational IR bands of methane [14–21]. Most of the published works make use of incoherent light FTIR or grating spectroscopy [14–16] to derive methane line parameters. Pine was the first to investigate methane ν_3 band line parameters [17,18] using narrow-linewidth MIR tunable laser sources, namely a difference-frequency (DFG) laser based on non-linear down-conversion of two visible dye lasers [22,23]. Despite the micro-watt level MIR power available from DFG lasers, Ghysels et al. recently performed in-situ measurement of the temperature dependence of the air-broadening, air-narrowing and line-mixing coefficients of the $R(6)$ manifold of the ν_3 band of CH_4 using a compact commercial DFG spectrometer [24]. Tunable MIR diode laser spectroscopy (TDLS, mostly using LN_2-cooled Pb-salt diode lasers) have also been recently used to investigate the temperature dependence of line mixing and N_2 pressure broadening parameters of the $P(9)$ multiplet components [19]. The N_2 pressure shift of the same $P(9)$ components and their temperature dependence have been investigated by Tumuhimbise et al. using TDLS [20]. Very recently, the room-temperature N_2-shift coefficients of the $P(7)$ to $P(11)$ components of $^{12}CH_4$ were measured by Vispoel et al. using a Pb-salt diode laser spectrometer [25]. Directly related to our work, some measurements on N_2-broadening and shift coefficients of $P(1)$, $R(0)$ and $R(1)$ lines in the ν_3 band of methane have been previously reported using FTIR [16] and DFG spectrometers [17,18].

It is thus interesting to compare the results of our measurements performed with a tunable cw OPO spectrometer with these previous works based on FTIR, Pb-salt or DFG laser spectrometers possessing the same spectral resolution. Because this work is also motivated by metrological traceability of spectral line parameter measurements to the SI unit, a special emphasis is made in the uncertainty evaluation of the retrieved broadening or shift coefficients, which is scarcely and sparsely documented in the literature. In order to avoid line mixing effects, we have chosen the 3 well-isolated singlet components of the strong ν_3 band, although the $P(1)$ line measurements may be contaminated at high pressure by the presence of a weak component of the $Q(10)$ line at 3008.988373 cm^{-1}. For this line the range of pressure was limited to ~300 Torr to limit the overlap with the satellite component.

2. The spectrometer platform

The spectrometer layout is depicted in Fig. 1, and is almost the same as the one used for line strengths measurements of CH_4 [8]. We thus only briefly summarize here the main parts of the OPO spectrometer. An external-cavity diode laser (ECDL, New Focus Velocity™ Widely Tunable Laser, model 6321), seeding a 10 W polarization-maintaining Yb:fiber amplifier (Yb-FA, Keopsys S.A.), is used to pump the singly-resonant OPO (SRO) configured as a bow-tie travelling-wave oscillator for the resonant signal-wave ($1450 < \lambda_s < 1650$ nm). The nonlinear crystal used to down-convert the pump photons into the mid-IR is a 5% magnesium-oxide-doped periodically-poled congruent lithium niobate (ppMgCLN, HC Photonics Corp., dimensions $16(W) \times 1(T) \times 50(L_c)$ mm^3). Only the grating period $\Lambda = 30.5$ μm of the multi-grating chip is used to phase-match ($T_{ppMgCLN} \sim 102$ °C) an idler wave output at $\lambda_i \sim 3.3$ μm for a pump wavelength near $\lambda_p = 1064$ nm. An intra-cavity thin YAG etalon helps to contend the occurrence of signal mode hop events intrinsic to low-gain cw parametric oscillators (such events are monitored by a scanning Fabry–Pérot interferometer, FPI, analyzing the leaking signal wave output). Another (non-scanning) FPI with a nominal free-spectral range FSR = 1.5 GHz (Thorlabs SA200-8B), finesse F ~ 250 at 1064 nm, analyzes the spectrum of the phase-modulated pump laser during pump frequency scans over < 10 GHz performed via the piezo-transducer (PZT) controlling the extended-cavity length of the ECDL. The phase-modulated sidebands, created by an electro-optic phase modulator (EOM, New Focus Model 4001) driven at $f_{RF} = 30$ MHz, provide ±30 MHz frequency markers allowing an absolute frequency calibration of the idler scan (in a cw SRO, the pump scan is entirely transferred to the idler wave, keeping the oscillating signal wave frequency unchanged [6–8]). However because the signal-wave of the SRO is not frequency-stabilized as in [4,6], the short-term idler linewidth is not limited by the pump laser short-term linewidth ($\Delta\nu_p < 300$ kHz) but determined by the signal mode jitter (typically < 5–13 MHz in 1 s in such SROs).

The idler beam from the OPO ($P_i \sim 0.3$–0.4 W when the OPO is pumped 2 times above its $P_{th} = 3$ W threshold), filtered from the residual pump and leaking signal wave by a dichroic beamsplitter (DBS, $R_{p,s} > 99.9\%$), is split into two channels so as to synchronously record the idler intensity baseline and the power transmitted by the cell. For a well-behaved laser (not subject to frequent mode-hops such as a cw OPO), the intensity base line used to compute the absorbance $-\ln[[I(\nu)]/I_0]$ does not vary in time and can be recorded once and for all with the empty cell. In our spectrometer, because the idler mode in resonance with the molecular line may correspond to different pump/signal modes of the OPO, the resulting idler intensity may fluctuate from one measurement to another, hence the necessity to synchronously monitor the transmitted intensity and its corresponding baseline by splitting the beam into 2 channels. The *spectroscopic channel* comprises a $L = 10$ cm-long gas cell equipped with tilted BaF_2 windows whose transmission is monitored by an InAs pin-photodiode (PD). The transmitted signals are attenuated to less than 1 mW with ND filters so as to remain within the linearity response zone of each photodiode. For the pressure broadening investigation the *reference channel* (without any pure CH_4 cell, see Fig. 1) simultaneously records the baseline of the idler affected by residual fringes (see Fig. 2) originating from etalon effects due to the poor AR-coating of the ppMgCLN facets in the idler range (the fringe period equals $c/2nL_c = 1.36$ GHz where $n = 2.2$ and $L_c = 50$ mm are the refractive index and length of the chip).

For the pressure shift measurements, a reference cell with length L containing low pressure ($P = 1$ Torr) pure

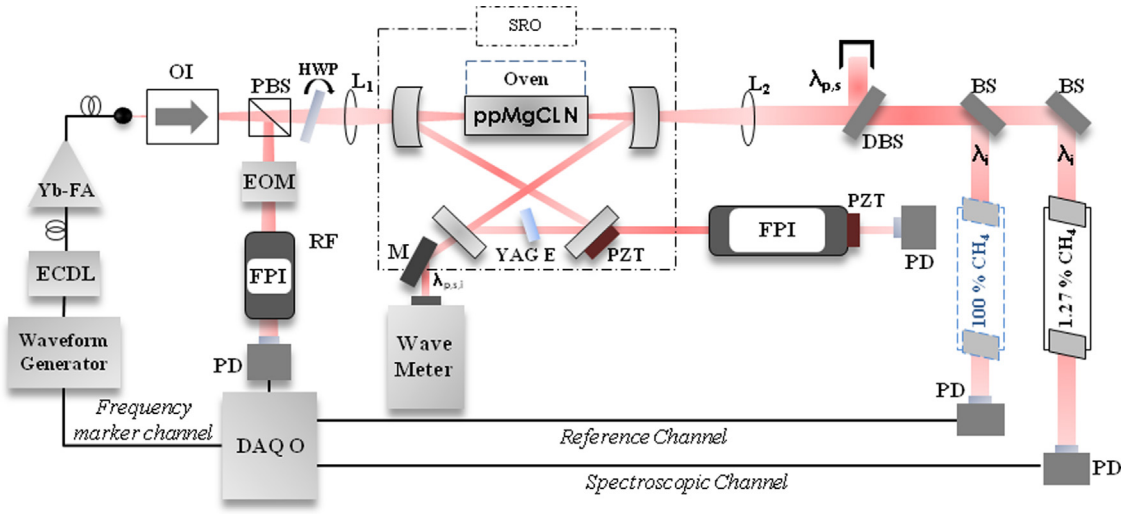

Fig. 1. Schematic of the OPO spectrometer. OI: optical isolator, PBS: polarizing beam splitter cube, HWP: half-wave plate, BS: beam splitter, L: lens, PD: photodetector, DAQ O: digital oscilloscope. The remaining labels are explained in the text. For the pressure shift measurements, a second identical gas cell (sketched in blue dash) is placed on the reference channel path. (For interpretation of the references to color in this figure legend, the reader is referred to the web version of this article.)

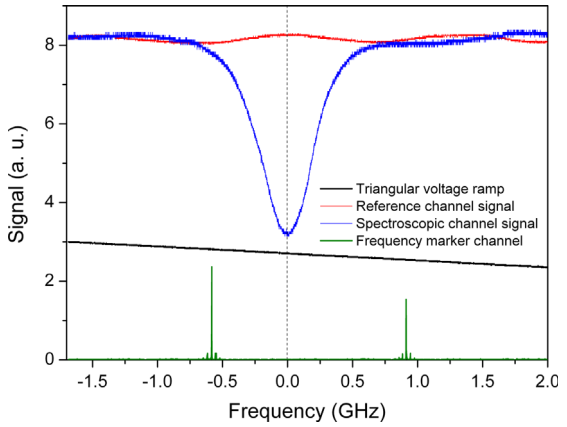

Fig. 2. Data acquisition of the CH_4 $R(0)$ transition located at 3028.752175 cm^{-1} at a pressure of 50 Torr for the spectroscopic channel (blue curve). Each trace is sampled with 10,000 points. The reference channel (red curve) represents the idler baseline (without the pure CH_4 reference cell in Fig. 1). The Frequency Marker channel (green curve showing two successive Fabry–Pérot phase-modulated pump fringes) allows the conversion of the oscilloscope time axis into relative frequency axis. The black curve corresponds to the triangular voltage ramp applied to the PZT of the pump laser. (For interpretation of the references to color in this figure legend, the reader is referred to the web version of this article.)

methane (sketched with dashed line in Fig. 1) is inserted in the *reference channel* to provide a reference frequency ν_R. The N_2-pressure-shifted line center position $\nu_c(P)$ synchronously recorded through the *spectroscopic channel* is then compared to the latter in order to determine the corresponding collision-induced shift ($\Delta\nu(P)=|\nu_c(P)-\nu_R|$). This relative method was adopted because the accuracy of the wavemeter ($\pm$60 MHz at 3 μm) was not sufficient to track the small shift ($\Delta\nu(P)<200$ MHz) from ~5 Torr – minimum

Table 1
SRO idler wavelength as a function of the ppMgCLN crystal's temperature and pump wavelength. Although the $P(1)$ line could be accessed at the same $T=102$ °C temperature as for $R(0)$ and $R(1)$ by setting the pump wavelength to 1067 nm, due to the decrease of spectral gain of the Yb-fiber amplifier beyond 1067 nm, another phase-matching combination (λ_p, T) was chosen so as to keep the pump laser near 1064 nm.

Pump wavelength (nm)	Temperature of the ppMgCLN crystal (°C)	Wavenumber (cm^{-1})	CH_4 lines	Line symmetry
1064.0	102	3028.752175	$R(0)$	A1
1063.7	102	3038.498427	$R(1)$	F1
1064.2	90	3009.011267	$P(1)$	F1

detectable absorption of the 1.27% $^{12}CH_4$:N_2 mixture – to atmospheric pressure.

In order to match as closely as possible the idler wavelength to the targeted CH_4 line positions (documented in HITRAN [26] and listed in Table 1), the idler wavenumber is monitored with a Michelson-interferometer-based wavemeter (Bristol Instruments model 621B-IR, with a 10^{-6} relative accuracy). The pump wavelength is used to tune the idler across the molecular line. When the readout of the wavemeter matches the line position wavenumber, the idler frequency is then fine-scanned over ~10 GHz using a triangular voltage ramp (at 1–3 Hz rate), capturing thus the target line profile which is displayed on a digital oscilloscope (DAQ O in Fig. 1, Lecroy Wavejet 334A, 2 GS/s). The signals coming from the reference and frequency-marker channels are synchronously recorded by the oscilloscope which is triggered by the scanning voltage ramp. When a signal mode-hop inadvertently occurs, the spectroscopic pattern can be retrieved by just a manual voltage-bias change applied (via a high-voltage amplifier, not shown in Fig. 1) to the PZT actuator attached to one of the OPO plane

Table 2
Measurement conditions for pressure broadening and shift determinations at $T=296$ K. The gas sample of 1.27% CH_4/N_2 was set in a $L=10$ cm-long gas cell. The range of pressure for $P(1)$ transition was limited to ≤ 300 Torr in order to limit the overlap with the weak satellite line.

CH_4 lines	Pressure broadening measurements (Torr)	Pressure shift measurements (Torr)
***R*(0)**	$P=25$–700	$P=44$–760
***R*(1)**	$P=50$–800	$P=130$–600
***P*(1)**	$P=50$–300	$P=50$–300

mirrors, restoring either the initial oscillating signal mode or an adjacent one.

To investigate the N_2-pressure broadening and shift coefficients from direct absorption spectroscopy, a gas mixture of 1.27% CH_4 (99.99% natural abundance purity) in nitrogen in-house prepared using the gravimetric technique was used. This gas sample was set in a $L=10$ cm-long absorption cell placed in the *spectroscopic channel* (Fig. 1). The measurements were made at different pressures varying between $P=25$ and $P=800$ Torr according to the studied line (Table 2).

3. Assessing the influence of the fringed baseline on the line parameter retrieval

Fig. 2 shows a typical synchronous recording of the photodiode signals corresponding to the various channels depicted in Fig. 1 for the $R(0)$ line at a pressure $P=50$ Torr.

The frequency marker trace (transmission of the pump Fabry–Pérot interferometer with nominal free-spectral-range FSR=1.5 GHz, bottom trace in Fig. 2) displays two successive pump fringes flanked with two phase-modulated side-bands at $\pm f_{RF}=\pm 30$ MHz. We used the $\pm f_{RF}$ frequency markers to statistically calibrate the FSR of the interferometer, yielding an average FSR=(1500 ± 15) MHz when the pump scan rate is 1–3 Hz. This $\pm 1\%$ uncertainty in the frequency axis calibration is obtained when the pump laser scan rate is slow enough (1–3 Hz), minimizing the PZT nonlinearity. Besides the PZT nonlinearity, the oscillating signal mode jitter also contributes to the residual uncertainty in the MIR frequency calibration because of energy conservation ($\nu_p=\nu_s+\nu_i$) in the parametric downconversion process.

The top (red) curve displaying a fringed background is the signal detected on the reference channel path (plotted for clarity with an inverted sign with respect to the transmitted $R(0)$ line trace in blue). As already stated in Section 2, the fringes originate from the idler etalon effect due to the intracavity ppMgCLN crystal. The modulated idler baseline can be accurately fitted to the transmission of a low-finesse Fabry–Pérot etalon, $I_{base}(\nu)=I_0[1+a_1\sin^2(a_2\nu+a_3)]$. It is thus important to assess the influence of the fringed baseline on the molecular transition linewidth and shift accuracy, since no preliminary intensity stabilization of the idler output was done to provide a flat baseline.

The gas cell transmitted intensity follows the Beer–Lambert law,

$$I(\nu)=I_{base}(\nu)\times\exp\left(-\alpha(\nu-\nu_c)L\right) \quad (1)$$

where ν_c is the center line frequency, L is the absorption path length, and the absorption coefficient $\alpha(\nu)=S(T)g(\nu-\nu_c)n$ is proportional to the line strength $S(T)$ [8], normalized lineshape (Voigt profile) $g(\nu-\nu_c)$, and to the absorbing molecule density n. The collisional broadening coefficient is defined as the slope of the plot of the Lorentzian half-linewidth (HWHM) of the absorbance profile versus pressure P, the absorbance being defined as $A(\nu)=\alpha(\nu-\nu_c)L$. Taking the natural logarithm of the transmitted intensity from which the small non-zero electronic offset of the photodetector is subtracted leads to

$$\ln[I(\nu)]=\ln(I_0)+\ln[1+a_1\sin^2(a_2\nu+a_3)]-\alpha(\nu-\nu_c)L \quad (2)$$

We used the general Voigt function $V(\nu;\nu_c,\gamma_D,\gamma_L,y_0,y_1)=y_0+y_1\,g(\nu-\nu_c;\gamma_D,\gamma_L)$ of Origin© software to fit the logarithm of the experimental data to a user-defined function, $F(\nu)=V(\nu;\nu_c,\gamma_D,\gamma_L,y_0,y_1)+\ln[1+a_1\sin^2(a_2\nu+a_3)]$, in order to account for the baseline modulation. Note that the Gaussian (Doppler) width (γ_D) and Lorentzian width (γ_L) parameters are defined as FWHM in the software. Up to 1000 experimental data points per fitted trace are used to derive all the fit parameters. In some cases when the fit returns unrealistic values for γ_D, the Doppler width was fixed to its theoretical value. Fig. 3 shows the result of the absorbance fit (natural logarithm of the transmittance data of Fig. 2) taking into account the baseline modulation (black line labeled (2)) is compared to the fit with a flat baseline (pink line labeled (1)). It appears that the experimental data (hollow circles) are well fitted by the above user-defined function especially in the wings of the spectrum, with corresponding fit residuals plotted in panel (b). The Lorentzian width derived from the fits are respectively $\gamma_L=200.12$ MHz (with modulation) and $\gamma_L=202.80$ MHz (without modulation).

It follows then that the uncertainty due to the baseline modulation on the determination of the collisional broadening is about $\pm 1\%$, much less than the uncertainty due to the relative frequency calibration and to the dispersion due to the trace-to-trace repeatability of the spectrum recording (Section 4). For each pressure setting, 10–15 spectra were acquired, fitted, and the resulting line parameter (broadening

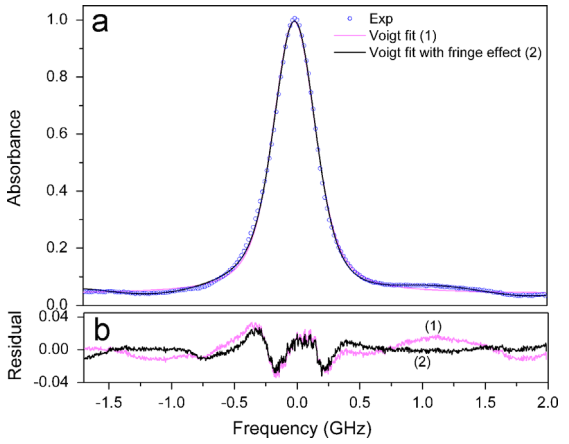

Fig. 3. Comparison of absorbance least-square fit of the $R(0)$ line data in Fig. 2 ($P=50$ Torr) with (2) or without (1) idler baseline modulation. (For interpretation of the references to color in this figure legend, the reader is referred to the web version of this article.)

or shift) statistically averaged. From the inspection of the fit residual shape, a fitting model including speed-dependent effects may improve the accuracy of the derived Lorentzian width; however due to the experimental systematic effects affecting the noise level of the OPO spectrometer we have opted for a simple Voigt profile to model our spectra.

A possible origin of the small trace-to-trace recording fluctuations affecting the measurement repeatability may be the residual frequency jitter of the resonant signal wave of the free-running OPO (typically $\Delta\nu_{\text{jitter}} \leq 13$ MHz on a $\sim$1 s timescale for a signal-resonant OPO, [27]) coupled with the slow scan rate (1–3 Hz) – chosen so as to minimize the PZT nonlinearity of the pump scan but not favorable with respect to the jitter time scale. Another possible explanation is related to the occurrence of signal wave mode hop events during the acquisition period of the $\sim$15 spectra samples per pressure setting (not all spectra were recorded with the same signal mode). Given that the idler power of the OPO may vary by $\sim$30% depending on the signal mode, the transmitted power detected by the InAs photodiode may fluctuate from one recording to another, addressing the power linearity issue of the photodiode and introducing a fluctuation in the signal-to-noise ratio. As to the possible power broadening of the molecular transition, it can be completely ruled out with the idler power level used.

4. Pressure broadening coefficients

In the presence of a foreign buffer gas, when one neglects self-broadening effects, the pressure broadening coefficient, noted γ_L^0 (in $\text{cm}^{-1}\,\text{atm}^{-1}$), is defined as the slope of the linear variation of the HWHM absorbance Lorentz width versus total pressure,

$$(1/2)\gamma_{\text{L}}(\text{FWHM}) = \gamma_L^0 P. \quad (3)$$

In Fig. 4 we show the histogram of 99 independent determinations of $R(0)$ pressure broadening coefficient calculated from Eq. (3) with a typical uncertainty of 0.5% originating from the non-linear fitting procedure (Levenberg–Marquardt) of the absorbance spectra. The data are obtained for a total pressure inside the sample gas cell ranging between 25 and 700 Torr, at temperature $T=296$ K. Dispersion in the results, mainly originating from measurements repeatability, presents a relative standard deviation (1σ) of 2.6%. (i.e. $\sim$5 times larger than the statistical uncertainty extracted from the fitting routine) when fitting the histogram with a normal distribution. Thus, statistical uncertainty is not the limiting factor in the total uncertainty budget.

The main sources of systematic errors in our experiment originate from both uncertainties on the frequency-scale calibration (affecting the HWHM absorbance Lorentz width) and on the pressure determination. In order to account for these sources of errors we estimated the uncertainties on both parameters. The pressure inside the sample cell is measured by a Baratron© capacitive gauge. Because the pressure gauge is not attached directly to the sealed gas cell, but located upstream, the pressure value is the readout from the gauge unit just after the cell valve is closed, thus the relative uncertainty on the pressure measurement is estimated to be 2% of the total pressure. The relative uncertainty on the frequency scale calibration is estimated to be at least 1% of the measured FSR of the pump Fabry–Perot (i.e., $\pm$ 15 MHz$\sim 0.5\times10^{-3}\,\text{cm}^{-1}$).

The determination of the $R(0)$ pressure broadening coefficient was finally derived from the slope of a weighted linear regression taking into account the errors on both parameters (York algorithm, [28]). During data analysis, it occurred that for some spectra sampling the fit returns an unrealistic value for the FWHM Doppler width γ_{D}. For such cases γ_{D} was fixed to the theoretical value $\gamma_{\text{D}}=\nu_c\sqrt{8k_BT\ln(2)/mc^2}\sim 280$ MHz, where ν_c is the line center frequency, k_B is the Boltzman constant, T (in K) is the temperature, m is the molecular mass of CH_4 and c the speed of light.

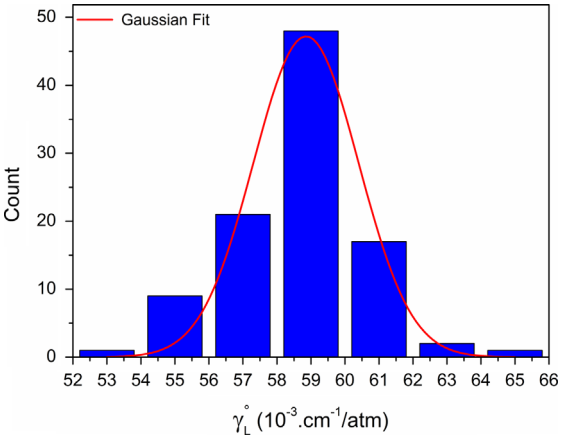

Fig. 4. Histogram of 99 independent determinations of the $R(0)$ line broadening coefficient γ_L^0 calculated from Eq. (3) for a pressure in the sample gas cell varying between 5 and 800 Torr, and temperature $T=296$ K. The expected value obtained from the Gaussian fit (red curve) is $58.85\times10^{-3}\,\text{cm}^{-1}\,\text{atm}^{-1}$ with a standard deviation of $1.54\times10^{-3}\,\text{cm}^{-1}\,\text{atm}^{-1}$. (For interpretation of the references to color in this figure legend, the reader is referred to the web version of this article.)

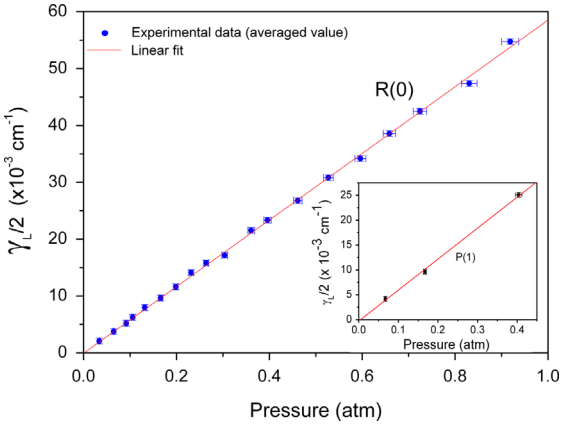

Fig. 5. HWHM absorbance Lorentz width $\gamma_L/2$ of the $R(0)$ (main frame) and $P(1)$ (inset) $^{12}CH_4$ transition as a function of pressure. Each point is the average of $\sim$10–15 independent measurements. The intercept of the best-fit line with the vertical axis is -0.08 ± 0.59 ($\times10^{-3}\,\text{cm}^{-1}$) for $R(0)$ ensuring almost no systematic (offset) errors. The intercept value for $P(1)$ fit is -0.28 ± 0.56 ($\times10^{-3}\,\text{cm}^{-1}$).

Fig. 5 represents the Lorentzian absorbance half-width $\gamma_L/2$ for the $R(0)$ transition as a function of total pressure (the inset figure shows the same plot for $P(1)$). The error bars shown in Fig. 5 correspond to the uncertainties on both the pressure and frequency-scale calibration respectively. We have expressed the frequency unit in wavenumber (cm^{-1}) and the pressure unit in atm (1 atm=760 Torr) to be consistent with the standard pressure broadening coefficient unit in (cm^{-1} atm^{-1}) used in HITRAN database.

The final value of the N_2-broadening coefficient of the $R(0)$ transition inferred from the fit was $\gamma_L^0=0.05863\pm 0.00037$ cm^{-1} atm^{-1}. The associated uncertainty of 3.7×10^{-4} cm^{-1} atm^{-1} corresponds to the standard error ($\pm\sim0.63\%$) on the estimation of the slope given by the least square fitting algorithm. Let us note that the retrieved slope value is very close to the mean value of the coefficient determined from the histogram in Fig. 4. The 1σ width of the Gaussian distribution ($\pm2.6\%$) could be inferred as a conservative upper-bound uncertainty on the pressure broadening coefficient, if all experimental systematic effects were to be taken into account.

The same data analysis was performed to determine the N_2 broadening coefficients of $R(1)$ and $P(1)$ transitions. The results are presented in Table 3 and compared with previously published determinations from Benner et al. [16], Pine [17] and Pine and Gabard [18]. A graphical comparison of the published results for the measured singlet lines is further shown in Fig. 6. It can be noticed that for $R(0)$ (filled squares) the broadening coefficients agree rather well and are closely distributed around a mean value 59.3×10^{-3} $cm^{-1}atm^{-1}$, although the individual reported uncertainty bars do not overlap (the uncertainty budget in the quoted references are hardly documented however, and the small attributed uncertainties correspond rather to statistical fit uncertainties not taking into account all systematic effects). Similarly the 4 coefficients for $R(1)$ are equivalently in good agreement around a mean value 65.1×10^{-3} cm^{-1} atm^{-1}. Note that Benner et al. [16] measured these broadening coefficients in 1993 using a Fourier transform spectrometer with a limited $\sim10^{-2}$ cm^{-1} resolution and that they were retrieved from the best non-linear least square fitting routine of the absorption lines assuming a Voigt lineshape. In Pine [17] broadening coefficients were obtained using a DFG spectrometer based on the difference-frequency of two dye-lasers with a $\sim$1–5 MHz resolution. In this last work the absorption lines were fitted assuming a Rautian profile taking into account narrowing of the Doppler broadened line due to collisions (the Dicke effect). The latter work was reinvestigated in 2000 by Pine and Gabard [18] considering a more elaborated theoretical line profile including speed dependent broadening and line mixing effects. The new values they found for $R(0)$ and $R(1)$ were $\sim$3% larger than their 1997 results, but they did not list the broadening coefficient of $P(1)$ in their table. Our values for $R(0)$ and $R(1)$ are found closer to those given in [17] (-1.7% and -1.3% discrepancy) than to their updated ones [18] using speed-dependent line mixing profile model which, for these well-isolated R-line singlets, may be superfluous. Direct comparison with HITRAN 2012 data is not straightforward because only line-by-line γ_L^0(air) values are listed in the database. Recently however some ab-initio Complex Robert–Bonamy (CRB) calculations of N_2 line broadening in the entire ν_3 band established the ratio γ_L^0 (air)/γ_L^0 (N_2) ≈ 0.98 for low J'' rotational quantum numbers [29]. Using this relation for the $R(0)$ and $R(1)$ air-broadened coefficients of HITRAN yields respectively 0.0583- and 0.0645-cm^{-1} atm^{-1} (with 5–10% uncertainty), again very close to our value in Table 3.

As to $P(1)$ broadening coefficient, we could find only the value listed by Pine [17] for direct comparison (the P-branch list of updated Pine and Gabard coefficients [18] contains only lines with $J''\geq2$). Regarding the two R-branch lines, the discrepancy with Pine [17] value for $P(1)$ broadening coefficient ($+4.3\%$) is slightly larger. We however note that in the latest ab-initio Robert–Bonamy (RB) calculations of ν_3 band nitrogen broadening by Gabard and Boudon [30], our $P(1)$ value matches closely their theoretical value plotted in their Fig. 4 (~0.060 cm^{-1} atm^{-1}). It is however worth mentioning that the overall trend in their calculations shows that the theoretical N_2-broadening coefficients for the lines belonging to the ν_3 band of methane are $\sim$5–10% smaller when

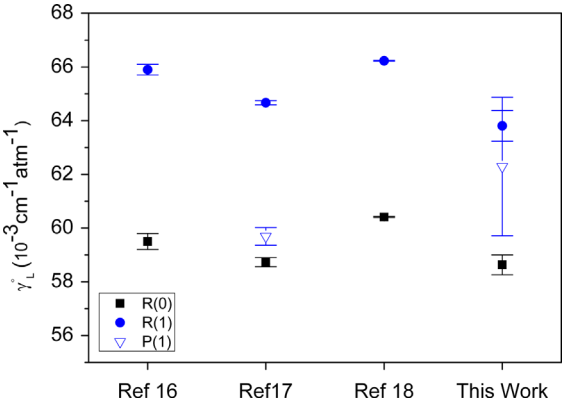

Fig. 6. Comparison of published N_2-pressure-broadening γ_L^0 values for $R(0)$, $R(1)$ and $P(1)$ CH_4 transitions with ours. The uncertainty bars are the statistical uncertainty derived from the fit.

Table 3
Comparison between measured N_2-broadening coefficients (γ_L^0, in cm^{-1} atm^{-1}) of CH_4 in the ν_3 band. Numbers in parenthesis express the uncertainty as one standard deviation in units of the last digits.

CH_4 transitions	ν_0 (cm^{-1})	γ_L^0 (cm^{-1} atm^{-1})			
		Ref. [16]	Ref. [17]	Ref. [18]	This Work
***P*(1)**	3009.011406	–	0.05969 (33)	–	0.06229 (258)
***R*(0)**	3028.752260	0.0595(3)	0.05873 (17)	0.06041(2)	0.05863 (37)
***R*(1)**	3038.498494	0.0659(2)	0.06467 (8)	0.06623(2)	0.06381 (57)

compared to all experimental data (including [18]). Finally using the HITRAN air-broadened coefficient (0.0646 $cm^{-1}\,atm^{-1}$) and the ratio $\gamma_L^0(air)/\gamma_L^0(N_2)\approx 0.98$ in [29] one derives an expected nitrogen-broadened coefficient 0.0659 $cm^{-1}\,atm^{-1}$ ($\pm$10%), which is again compatible with our value to within the uncertainty bars. The larger uncertainty on our $P(1)$ coefficient is due to the limited range of pressure ($P<300$ Torr) to avoid interference with the weak line belonging to the tail of the Q-branch, and to the poorer signal-to-noise ratio of the recorded spectra. Further independent measurements for $P(1)$ coefficient over a larger pressure range and using a multi-line analysis including the neighboring weak $Q(10)$ component are needed to improve the accuracy of $P(1)$ broadening coefficient.

5. Pressure shift coefficients

To measure the pressure shift, estimated from published coefficients [16–18] to be ~150 MHz from zero to atmospheric pressure, the use of the wavemeter whose absolute accuracy (+/−60 MHz at 3 μm) is insufficient is precluded even by actively stabilizing the idler wave of the OPO on top of the pressure-broadened transmission profile. Thus, the determination of such small pressure shift requires a relative method where a second cell filled with low-pressure pure CH_4 serves as a reference frequency, as done for the measurements of the lineshift of $P(7)$, $P(10)$ and $P(11)$ multiplets in nitrogen [25].

Thus, an identical 10-cm long gas cell filled with pure CH_4 at low-pressure ($P_R\sim 1$ Torr, Doppler regime) was added to the optical setup shown in Fig. 1. The new cell, labeled reference cell, was placed in front of the PD corresponding to the reference channel in order to provide the reference absorption line. More precisely, we are interested by the central value "ν_c" of the experimental absorbance corresponding to the absorption peak. Therefore, the principle of measurement of the N_2-pressure-induced shift of the line center frequency consists hence in synchronously recording the Doppler-broadened absorbance lineshape of the reference sample (with line center position at $\nu_R=\nu_0+\delta^0_{CH_4}P_R$ where ν_0 is the unperturbed, i.e. zero pressure, methane line transition and $\delta^0_{CH_4}$ the self-shift coefficient) together with the transmitted absorbance lineshape of the CH_4:N_2 sample (with line center $\nu_c(P)=\nu_0+\delta^0_{CH_4}xP+\delta^0_{N_2}(1-x)P$, P being the total pressure of the gas mixture in the sample cell and $x=1.27\%$ being the amount fraction of the absorbing gas). The two lineshapes are then fitted to a Voigt profile, yielding the relative positions of the two line centers by measuring the spacing,

$$\Delta\nu(P)=\nu_c(P)-\nu_R\approx\delta^0_{N_2}P. \quad (4)$$

Here we have neglected the much smaller contribution of the term $(\delta^0_{CH_4}-\delta^0_{N_2})xP-\delta^0_{CH_4}P_R$ in the frequency difference to retrieve the linear dependence on the total pressure.

During the measurements, the spectroscopic gas cell was filled with the same gas mixture as used for the pressure broadening measurements. The pressure inside the cell was varied between 60 and 760 Torr depending on the targeted transition (for $P(1)$ the pressure range was limited to ~300 Torr due to the presence of the nearby weak $Q(10)$ transition). In order to determine $\Delta\nu(P)$, the reference cell was filled with pure natural abundance CH_4 at a fixed pressure of $P_R=1$ Torr (1.318×10^{-3} atm) at which the reference cell absorption amounts to ~90%. Typically, up to 10 spectra were recorded for each pressure setting in order to get a statistical average of the measured $\Delta\nu(P)$. The two synchronously recorded absorbance spectra are then fitted with a Voigt profile to determine the difference frequency of their line centers.

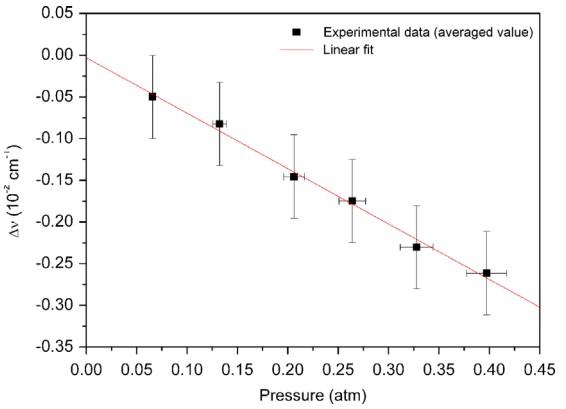

Fig. 7. Line center frequency difference $\Delta\nu=\nu_c(P)-\nu_R$ between the N_2-shifted frequency and the pure methane ($P_R=1$ Torr) reference frequency for the $P(1)$ line located at 3009.011297 cm^{-1} as a function of the pressure. The straight line is the linear regression of the experimental data.

Finally, by plotting $\Delta\nu$ (in cm^{-1}) as a function of the total pressure (in atm), Fig. 7, the pressure-induced frequency shift coefficient $\delta^0_{N_2}$ (in $cm^{-1}\,atm^{-1}$) could be deduced from the slope of a weighted linear fit of the data, taking also into account uncertainties on frequency (5×10^{-4} cm^{-1}) and pressure (2% of total pressure) [28]. As expected for the ν_3 band lines the shift is found negative.

The deduced slope from the fitted data in Fig. 7 for the $P(1)$ transition of CH_4 is equal to $\delta^0_{N_2}=(-0.00665\pm0.00007)$ $cm^{-1}\,atm^{-1}$ where the uncertainty (~1%) corresponds to the standard error on the estimation of the slope given by the least square fitting routine. The value of the intercept of the straight line is as small as -0.003 (10^{-2} cm^{-1}), which justifies the neglect of the small contribution of self-shift in both the pure and the diluted binary mixture. Let us note that the relative uncertainty on the shift coefficient of $P(1)$ is smaller than the one related to the broadening coefficient in Table 3: the determination of line centers (ν_c) from the fit is much less sensitive to absorbance lineshape distortions than the determination of γ_L.

Table 4 and Fig. 8 summarize our determined N_2-induced pressure shifts coefficients for $P(1)$, $R(0)$ and $R(1)$ CH_4 transitions that are compared with Ref. [16–18]. A rather fair agreement with Refs [17,18] is again found for $R(0)$ and $R(1)$ shift coefficients, although our $R(0)$ shift coefficient is slightly larger in magnitude. Based on the values listed in Table 4, and setting as the reference the mean value of the pressure shift coefficients determined in [16–18] we can infer for the $R(1)$ and $R(0)$ pressure shift coefficient a mean relative difference of −3.7% and +9.2% respectively. For the

Table 4
Comparison between measured N_2-induced pressure shifts coefficients (in $cm^{-1}\,atm^{-1}$) of CH_4 in the ν_3 band. Numbers in parenthesis express the uncertainty as one standard deviation in units of the last digits.

CH_4 transitions	ν_0 (cm^{-1})	$\delta^0_{N_2}$ ($cm^{-1}\,atm^{-1}$)			
		Ref. [16]	Ref. [17]	Ref. [18]	This work
***P*(1)**	3009.011406	–	−0.00721(14)	–	−0.00665(7)
***R*(0)**	3028.752260	−0.0062(0)	−0.00601(15)	−0.00620(1)	−0.00670(12)
***R*(1)**	3038.498494	−0.0050(1)	−0.00463(15)	−0.00486(1)	−0.00465(21)

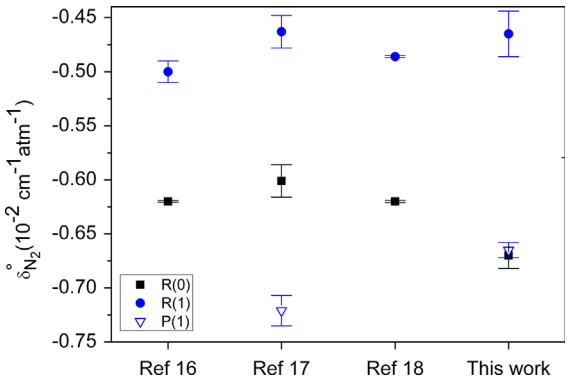

Fig. 8. Comparison of published N_2-pressure-shift coefficient $\delta^0_{N_2}$ for $R(0)$, $R(1)$ and $P(1)$ CH_4 transitions with ours. The uncertainty bars are the statistical uncertainty derived from the fit.

$P(1)$ pressure shift coefficient, the relative difference to [17] is found to be +7.7%. Finally we note that the HITRAN 2012 values of air-shifted coefficients for $P(1)$, $R(0)$ and $R(1)$ are given as, respectively, −0.00675, −0.00640 and $-0.00491\,cm^{-1}\,atm^{-1}$ (with an accuracy ≥ 0.001 and $< 0.01\,cm^{-1}\,atm^{-1}$). Given that $\delta^0_{air} \approx \delta^0_{N_2} \approx \delta^0_{O_2}$ for transitions in the ν_3 band of methane (Fig. 6 of Ref. [15] shows a comparison plot exemplified for a $P(8)$ component of $^{13}CH_4$), it is sound to compare our nitrogen shifts in Table 4 with the recommended values from the database. A fairly good agreement is then also noted.

6. Conclusions

We have re-measured the nitrogen pressure-induced line broadening and shift of the 3 isolated singlet lines, $P(1)$, $R(0)$ and $R(1)$, of the ν_3 band of $^{12}CH_4$ around 3.3 μm by use of direct absorption spectroscopy performed with a tunable, continuous-wave, mid-IR singly-resonant optical parametric oscillator. The data analysis used to extract the broadening and shift coefficients is based on a simple Voigt profile model, with an emphasis on the uncertainty budget analysis which is affected by the numerous experimental biases – that are not often taken into account – inherent to experimental (nonlinear) laser spectroscopy. The overall uncertainty achieved for the broadening and shift coefficients is not limited by the statistical standard deviation of the fitting routine, but rather to experimental biases affecting the repeatability of the measurements. In our case, the broadening coefficients for $R(0)$ and $R(1)$ line are affected by a relative uncertainty of ~3% to account for the repeatability of the measurements, while for $P(1)$ line the uncertainty increases to ~5% due to partial interference with a satellite weak line of the Q-branch manifold. While the line shift coefficients for $P(1)$, $R(0)$, $R(1)$ derived from the data analysis display a relative statistical uncertainty below ~5%, estimating the numerous experimental biases which would expand the uncertainty is difficult. The reproducibility of the measurement of these spectroscopic parameters is checked by comparing our data with the previously published measurements performed using various spectroscopic instrumentation and line profile models. The comparison of experimental data shows that the broadening line data display a dispersion of up to ~10%, far above the associated uncertainties.

To reduce such discrepancies and improve the traceability to SI units of the measurement of spectroscopic line parameter data, improvements in the OPO spectrometer setup are required. An intensity stabilization of the idler beam would improve the shot-to-shot repeatability of the measurement. To reduce the uncertainty on the frequency scale, absolute frequency measurements instead of relative frequency calibration may be used by referencing (stabilizing) the OPO to e.g. a femtosecond frequency comb based on a mode-locked laser (such as an Er:fiber laser comb) as done in high-resolution spectroscopic setups [3–5]. With an absolute frequency scale traceable to the time/frequency standard, assessing the influence of the laser scan nonlinearity would be eased. Moreover, once the pump laser and signal-wave of the OPO are phase/frequency locked to the comb teeth (thus eliminating the signal mode frequency jitter of a free-running OPO), the comb repetition rate can be swept to obtain an accurate scan of the idler-wave [5]. The repeatability of the measurement should then be improved. Once all experimental biases are minimized and characterized, refined collision-induced line broadening and shift models will then help to reduce further the associated uncertainties.

Acknowledgments

The authors acknowledge partial support from a FP7-EURAMET grant (Contract no. ENV-06). M.P. Moreno thanks CAPES for postdoctoral fellowship support under BEX-12610-12-7. The authors thank the France-Brazil PHC-CAPES-Cofecub program (project code: 25060RE/710-11) for partial support.

References

[1] Kovalchuk EV, Dekorsy D, Lvovsky AI, Braxmaier C, Mlynek J, Peters A. High-resolution Doppler-free molecular spectroscopy with a

continuous-wave optical parametric oscillator. Opt Lett 2001;26:1430–2.
[2] Vainio M, Siltanen M, Peltola J, Halonen L. Grating-cavity continuous-wave optical parametric oscillators for high-resolution mid-infrared spectroscopy. Appl Opt 2011;50:A1–10.
[3] Vainio M, Merimaa M, Peltola J, Halonen L. Frequency-comb-referenced molecular spectroscopy in the mid-infrared region. Opt Lett 2011;36:4122–4.
[4] Ricciardi I, De Tommasi E, Maddaloni P, Mosca S, Rocco A, Zondy JJ, et al. A narrow-linewidth optical parametric oscillator for mid-infrared high resolution spectroscopy. Mol Phys 2012;110:2103–9.
[5] Ricciardi I, De Tommasi E, Maddaloni P, Mosca S, Rocco A, Zondy JJ, et al. Frequency-comb-referenced singly-resonant OPO for sub-Doppler spectroscopy. Opt Express 2012;20:9178–86.
[6] Andrieux E, Zanon T, Cadoret M, Rihan A, Zondy JJ. 500-GHz mode-hop-free idler tuning range with a frequency-stabilized singly resonant optical parametric oscillator. Opt Lett 2011;36:1212–4.
[7] Courtois J, Bouchendira R, Cadoret M, Ricciardi I, Mosca S, De Rosa M, et al. High-speed multi-THz-range mode-hop-free tunable mid-IR laser spectrometer. Opt Lett 2013;38:1972–4.
[8] Moreno MP, Cadoret M, Jahjah M, Nguyen L, Cruz FC, Zondy JJ. Line intensity measurements of methane's ν_3-band using a cw-OPO. (online first). Appl Phys B 2014;117:681–7. http://dx.doi.org/10.1007/s00340-014-5883-1.
[9] Pine AS, Gabard T. Multispectrum fits for line mixing in the ν_3 band Q branch of methane. J Mol Spectrosc 2003;217:105–14.
[10] Wuebbles DJ, Hayhoe K. Atmospheric methane and global change. Earth Sci Rev 2002;57:177–210.
[11] Brown RH, Baines KH, Bellucci G, Bibring JP, Buratti BJ, Capaccioni F, et al. Observations with the visual and infrared mapping spectrometer (VIMS) during Cassini's flight by of Jupiter. Icarus 2003;164:461–70.
[12] Webster CR. Measuring methane and its isotopes $^{12}CH_4$, $^{13}CH_4$, and CH_3D on the surface of Mars with in situ laser spectroscopy. Appl Opt 2005;44:1226–35.
[13] Lemonn MT, Smith PH, Lorenz RD. Methane abundance on titan, measured by the space telescope imaging spectrograph. Icarus 2002;160:375–85.
[14] Devi VM, Rinsland CP, Smith MAH, Benner DC. Air-broadened Lorentz halfwidths and pressure-induced line shifts in the ν_4 band of $^{13}CH_4$. Appl Opt 1988;27:2296–308.
[15] Devi VM, Benner DC, Smith MAH, Rinsland CP. Measurements of air-, N_2-, and O_2-broadened halfwidths and pressure-induced line shifts in the ν_3 band of $^{13}CH_4$. Appl Opt 1991;30:287–304.
[16] Benner DC, Devi VM, Smith MAH, Rinsland CP. Air-, N_2-, and O_2-broadening and shift coefficients in the ν_3 spectral region of $^{12}CH_4$. J Quant Spectrosc Radiat Transf 1993;50:65–89.
[17] Pine AS. N_2 and Ar broadening and line mixing in the P and R branches of the ν_3 band of CH_4. J Quant Spectrosc Radiat Transf 1997;57:157–76.
[18] Pine AS, Gabard T. Speed-dependent broadening and line mixing in CH_4 perturbed by Ar and N_2 from multispectrum fits. J Quant Spectrosc Radiat Transf 2000;66:69–92.
[19] Mondelain D, Payan S, Deng W, Camy-Peyret C, Hurtmans D, Mantz AW. Measurement of the temperature dependence of line mixing and pressure broadening parameters between 296 and 90 K in the ν_3 band of $^{12}CH_4$ and their influence on atmospheric methane retrievals. J Mol Spectrosc 2007;244:130–7.
[20] Tumuhimbise AT, Hurtmans D, Mondelain D, Mantz AW. Nitrogen-pressure shifts in the ν_3 band of methane measured at several temperatures between 300 and 90 K. J Mol Spectrosc 2008;252:239–41.
[21] Smith MAH, Benner DC, Predoi-Cross A, Devi VM. Air- and self-broadened halfwidths, pressure-induced shifts, and line mixing in the ν_2 band of $^{12}CH_4$. J Quant Spectrosc Radiat Transf 2014;133:217–34.
[22] Pine AS. Doppler-limited molecular spectroscopy by difference-frequency mixing. J Opt Soc Am 1974;64:1683–90.
[23] Pine AS. High-resolution methane v3-band spectra using a stabilized tunable difference-frequency laser system. J Opt Soc Am 1976;66:97–108.
[24] Ghysels M, Gomez L, Cousin J, Tran H, Amarouche N, Engel A, et al. Temperature dependences of air-broadening, air-narrowing and line-mixing coefficients of the methane ν_3 R(6) manifold lines—application to in-situ measurements of atmospheric methane. J Quant Spectrosc Radiat Transf 2014;133:206–16.
[25] Vispoel B, Dhyne M, Populaire JC, Blanquet G, Lepère M. N_2-shift coefficients in the ν_3 band of $^{12}CH_4$ at room temperature. J Mol Spectrosc 2014;298:7–10.
[26] Rothman LS, Gordon IE, Babikov Y, Barbe A, Chris Benner D, Bernath PF, et al. The HITRAN 2012 molecular spectroscopic database. J Quant Spectrosc Radiat Transf 2013;130:4–50. ⟨http://www.cfa.harvard.edu/hitran/download/hitran2012.pdf⟩.
[27] Müller F, von Basum G, Popp A, Halmer D, Hering P, Mürtz M, et al. Long-term frequency stability and linewidth properties of continuous-wave pump-resonant optical parametric oscillators. Appl Phys B 2005;80:307–13.
[28] York D. Least-squares fitting of a straight line. Can J Phys 1966;44:1079–86.
[29] Antony BK, Niles DL, Wroblewsky SB, Humphrey CM, Gabard T, Gamache RR. N_2-, O_2- and air-broadened half-widths and line shifts for transitions in the ν_3 band of methane in the 2726- to 3200-cm^{-1} spectral region. J Mol Spectrosc 2008;251:268–81.
[30] Gabard T, Boudon V. Line broadening coefficient calculations for methane perturbed by nitrogen. J Quant Spectrosc Radiat Transf 2010;111:1328–43.